

---

# Intriguing Properties of Contrastive Losses

---

**Ting Chen**  
Google Research, Brain Team  
iamtingchen@google.com

**Lala Li**  
Google Research, Brain Team  
lala@google.com

## Abstract

Contrastive loss and its variants have become very popular recently for learning visual representations without supervision. In this work, we first generalize the standard contrastive loss based on cross entropy to a broader family of losses that share an abstract form of  $\mathcal{L}_{\text{alignment}} + \lambda \mathcal{L}_{\text{distribution}}$ , where hidden representations are encouraged to (1) be aligned under some transformations/augmentations, and (2) match a prior distribution of high entropy. We show that various instantiations of the generalized loss perform similarly under the presence of a multi-layer non-linear projection head, and the temperature scaling ( $\tau$ ) widely used in the standard contrastive loss is (within a range) inversely related to the weighting ( $\lambda$ ) between the two loss terms.

We then study an intriguing phenomenon of *feature suppression* among competing features shared across augmented views, such as “color distribution” vs “object class”. We construct datasets with explicit and controllable competing features, and show that, for contrastive learning, a few bits of easy-to-learn shared features could suppress, and even fully prevent, the learning of other sets of competing features. Interestingly, this characteristic is much less detrimental in autoencoders based on a reconstruction loss. Existing contrastive learning methods critically rely on data augmentation to favor certain sets of features than others, while one may wish that a network would learn all competing features as much as its capacity allows.<sup>1</sup>

## 1 Introduction

Contrastive learning [1–14] has achieved great successes recently in learning unsupervised visual representations. As shown in [13, 14], contrastive learning can learn representations that rival supervised learning, and significantly improve state-of-the-art in semi-supervised learning on ImageNet. Despite its success, there is little understanding of its effectiveness or potential limitations.

One successful use case of contrastive loss for self-supervised learning is to make *augmented* views of the same example agree [1, 2, 13]. A widely used contrastive loss to encourage agreement is based on cross entropy [15, 3, 4, 13]. Given an augmented view of an example, the contrastive prediction task (via cross entropy loss) aims to classify a set of candidates into the positive example (i.e. the other augmented view of the same example) and negative ones. In this work, we first propose a generalization of this standard contrastive loss, and study its properties.

We then study the feature suppression phenomenon in contrastive learning. The suppression effect occurs among competing features shared across augmented views. For example, “color distribution” and “object class” are competing features as they are likely shared between two augmented views (when random cropping is used as the augmentation for certain datasets like ImageNet). In other words, these features constitute of mutual information bits between two augmented views. It has been shown that the existence of competing features like “color distribution” can significantly reduce the effectiveness of contrastive learning [13].

<sup>1</sup>Code at [https://github.com/google-research/simclr/tree/master/colabs/intriguing\\_properties](https://github.com/google-research/simclr/tree/master/colabs/intriguing_properties).

In order to study this phenomenon further in a quantitative manner, we propose two ways to construct datasets with explicit and controllable competing features. Our experiments show that shared features that are easy-to-learn, despite they only constitute a few bits of mutual information, could suppress, and even fully prevent, the learning of other sets of features. This phenomenon persists across different instantiations of the generalized contrastive loss, model sizes, as well as batch sizes (with or without memory), despite it is much less detrimental in autoencoders based on a reconstruction loss. We discuss some potential reasons that lead to the phenomenon, and note that existing contrastive learning methods [2, 6, 10, 13, 16] critically rely on hand-crafted data augmentation to favor certain sets of competing features than others.

**Organization.** Firstly, we propose the generalized contrastive loss and study its properties (section 2). Secondly, we construct datasets for studying “competing features” in contrastive learning (section 3).

## 2 Generalized Contrastive Loss

### 2.1 $\mathcal{L}_{\text{generalized contrastive}} = \mathcal{L}_{\text{alignment}} + \lambda \mathcal{L}_{\text{distribution}}$

Inspired by and built upon [17], we propose the following *abstract* form of generalized contrastive loss.

$$\boxed{\mathcal{L}_{\text{generalized contrastive}} = \mathcal{L}_{\text{alignment}} + \lambda \mathcal{L}_{\text{distribution}}} \quad (1)$$

Both terms are defined on hidden representations.  $\mathcal{L}_{\text{alignment}}$  encourages representations of augmented views to be consistent, while  $\mathcal{L}_{\text{distribution}}$  encourages representations (or a random subset of them) to match a prior distribution (of high entropy). In this section, we show that the standard contrastive loss based on cross entropy [15, 3, 4] is a special case, and also provide more instantiations of the generalized contrastive loss.

Following the notation in [13], we define the contrastive loss between two augmented views  $(i, j)$  of the same example for a mini-batch of size of  $n$ . The standard contrastive loss based on cross entropy can be written as the following.

$$\mathcal{L}^{\text{NT-Xent}} = -\frac{1}{n} \sum_{i,j \in \mathcal{MB}} \log \frac{\exp(\text{sim}(\mathbf{z}_i, \mathbf{z}_j)/\tau)}{\sum_{k=1}^{2n} \mathbb{1}_{[k \neq i]} \exp(\text{sim}(\mathbf{z}_i, \mathbf{z}_k)/\tau)} \quad (2)$$

where  $\mathbf{z}_i, \mathbf{z}_j$  are hidden representations of two augmented views of the same example,  $\text{sim}(\mathbf{u}, \mathbf{v}) = \mathbf{u}^T \mathbf{v} / (\|\mathbf{u}\| \|\mathbf{v}\|)$  is the cosine similarity between two vectors,  $\tau$  is a temperature scalar and  $\mathcal{MB}$  is a randomly sampled mini-batch consisting of augmented pairs of images. As shown in [13], the normalization and temperature scaling play an important role in the quality of learned representations, and make the standard contrastive loss somewhat different from standard cross entropy loss.

By expanding the loss and scaling it by a constant of  $\tau$ , we have:

$$\tau \mathcal{L}^{\text{NT-Xent}} = \underbrace{-\frac{1}{n} \sum_{i,j} \text{sim}(\mathbf{z}_i, \mathbf{z}_j)}_{\mathcal{L}_{\text{alignment}}} + \underbrace{\frac{\tau}{n} \sum_i \log \sum_{k=1}^{2n} \mathbb{1}_{[k \neq i]} \exp(\text{sim}(\mathbf{z}_i, \mathbf{z}_k)/\tau)}_{\mathcal{L}_{\text{distribution}}} \quad (3)$$

The minimization of the second term (i.e. the LogSumExp term) has an effect of matching the hidden representation to uniform distribution in the hypersphere, as previously shown in [17]. More specifically, the second term is closely connected to pairwise potential in a Gaussian kernel, and can be minimized with a perfect uniform encoder [17]. For this reason, we can consider it as a form of distribution matching loss, i.e. an instantiation of  $\mathcal{L}_{\text{distribution}}$ .

It is worth noting that  $\tau$  in Eq. 3 appears in two places, one as the scaling of the second term, and the other as the width of Gaussian kernel. They do not necessarily need to be the same, so we could decouple them as follows. The decoupling allows us to study the effects of them separately.

$$\mathcal{L}^{\text{Decoupled NT-Xent}} = -\frac{1}{n} \sum_{i,j} \text{sim}(\mathbf{z}_i, \mathbf{z}_j) + \lambda \frac{1}{n} \sum_i \log \sum_{k=1}^{2n} \mathbb{1}_{[k \neq i]} \exp(\text{sim}(\mathbf{z}_i, \mathbf{z}_k)/\tau) \quad (4)$$

Although the LogSumExp and the uniform hypersphere prior are widely used, partially due to the popularity of cross entropy loss, here we are interested in knowing *whether or not it is essential to the*

effectiveness of contrastive loss. Are there other priors that could also work (e.g. those in Figure 1)? And how much difference does it make by using other priors?

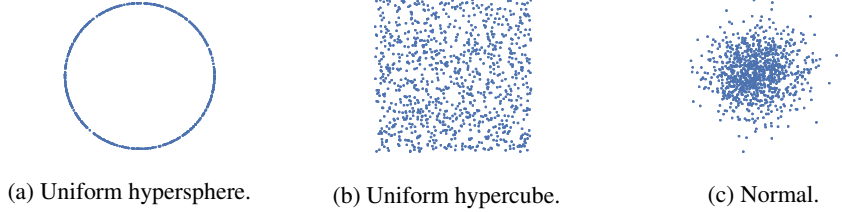


Figure 1: Examples of different prior distribution in 2-D space.

One issue of using other priors is we could not rely on LogSumExp for matching the distribution. To this end, we resort to the theory of optimal transport, via Sliced Wasserstein Distance (SWD) [18–20] in particular. For two sets of equal-sized samples from two 1-D distributions, the optimal transport can be obtained by computing two permutations that order the values of both sets of samples respectively. The 1-D Wasserstein distance can then be computed with  $\ell_2$  distance between the ordered values. For n-D distributions, we first project the samples to  $n$  randomly-generated orthogonal 1-D subspaces, and then compute and sum 1-D Wasserstein distance across all 1-D subspaces. By adjusting the network weights to minimize the SWD, we are able to reduce the mismatch between the distribution of hidden vectors and a known prior distribution. The detailed algorithm can be found in Algorithm 1.

---

**Algorithm 1** Sliced Wasserstein Distance (SWD) loss.

---

**input:** activation vectors  $\mathbf{H} \in \mathbb{R}^{b \times d}$ , a prior distribution (e.g. Gaussian) sampler  $\mathcal{S}$   
draw prior vectors  $\mathbf{P} \in \mathbb{R}^{b \times d}$  using  $\mathcal{S}$   
generate random orthogonal matrix  $\mathbf{W} \in \mathbb{R}^{d \times d'}$   
make projections:  $\mathbf{H}^\perp = \mathbf{H}\mathbf{W}$ ;  $\mathbf{P}^\perp = \mathbf{P}\mathbf{W}$   
initialize SWD loss  $\ell = 0$   
**for**  $j \in \{1, 2, \dots, d'\}$  **do**  
     $\ell = \ell + \|\text{sort}(\mathbf{H}_{:,j}^\perp) - \text{sort}(\mathbf{P}_{:,j}^\perp)\|^2$   
**end for**  
**return**  $\ell / (dd')$

---

With SWD loss, we are able to use a wider set of priors, including those in Figure 1, and potentially more. Table 1 summarizes instantiations of the generalized contrastive loss with different prior distributions and distribution matching loss.

Table 1: Instantiations of the generalized contrastive loss, i.e.  $\mathcal{L}_{\text{align}} + \lambda \mathcal{L}_{\text{distribution}}$ , that we considered in this work.  $\tilde{z}$  denotes  $\ell_2$ -normalized  $z \in \mathbb{R}^d$ .

$\mathcal{L}_{\text{align}}$	<b>Prior distribution</b>	$\mathcal{L}_{\text{distribution}}$
$\frac{1}{nd} \sum_{i,j} \ \tilde{z}_i - \tilde{z}_j\ ^2$	Uniform hypersphere	$\frac{1}{n} \sum_i \log \sum_j \exp(\tilde{z}_i^T \tilde{z}_j / \tau)$
$\frac{1}{nd} \sum_{i,j} \ \tilde{z}_i - \tilde{z}_j\ ^2$	Uniform hypersphere	SWD( $\tilde{Z}, Z^{\text{prior}}$ )
$\frac{1}{nd} \sum_{i,j} \ z_i - z_j\ ^2$	Uniform hypercube	SWD( $Z, Z^{\text{prior}}$ )
$\frac{1}{nd} \sum_{i,j} \ z_i - z_j\ ^2$	Normal distribution	SWD( $Z, Z^{\text{prior}}$ )

**Mutual Information.** The connection between the standard contrastive loss and mutual information has been shown before [3, 21], where the contrastive loss (a.k.a. InfoNCE loss [3]) is shown to be a lower bound of the mutual information. However, with the generalized contrastive loss, do we still have a similar connection?

The mutual information between two latent variables  $U, V$  can be expressed as

$$I(U; V) = H(U) - H(U|V) \tag{5}$$

Comparing this factorization of mutual information with generalized contrastive loss, it is not difficult to see that: (1) the alignment term  $\mathcal{L}_{\text{alignment}}$  is directly related to  $H(U|V)$  which aims to reduce uncertainty of the other views given one view of the example; and (2) the distribution matching term  $\mathcal{L}_{\text{distribution}}$  can be considered as a proxy to  $H(u)$  for maximizing the entropy in the representation. In particular, for representation in the hypersphere, the entropy is maximized if they are uniformly distributed [17]. It is perhaps worth noting that different from mutual information (Eq. 5), the generalized contrastive loss (Eq. 1) allows a tunable weight ( $\lambda$ ) between the alignment and distribution matching term, whose relation with the temperature ( $\tau$ ) in standard contrastive loss (Eq. 2) will be discussed later.

**Experimental setup.** We follow [13, 14] for the use of augmentations and architectures. By default, we use ResNet-50 [22] and a 2-layer projection head [13, 14] after the ResNet’s average pooling layer. We set the output ( $z$ ) dimensionality to 64 for CIFAR10 and 128 for ImageNet, since increasing them has little effect on the performance. The batch size and training epoch will be specified for each experiment. We use the linear evaluation protocol, i.e. the accuracy of a trained linear classifier on the learned features is used as a proxy for representation quality.

When comparing the standard contrastive loss (i.e. NT-Xent in Eq. 2) and other instantiations of the generalized contrastive loss (in Table 1), we optimize the hyper-parameters for different losses (for NT-Xent loss, we set  $\tau = 0.2$ ; for decoupled NT-Xent loss, we set  $\tau = 1.0, \lambda = 0.1$ ; for SWD based losses, we set  $\lambda = 5$ ; and since we use mean squared error instead of  $\ell_2$  distance in alignment loss for losses in Table 1, we find it helpful to scale the loss by 1000 when the hidden vector  $z$  is normalized). A batch size of 128 is used for CIFAR-10, and 1024 is used for ImageNet.

### 2.2 Different instantiations of the generalized contrastive loss perform similarly

Figure 2 shows linear evaluation results of models trained with different losses under different training epochs. On CIFAR-10, we see little differences in terms of linear evaluation for variants of the generalized contrastive losses, especially when trained longer than 200 epochs. As for ImageNet, there are some discrepancies between different losses, but they disappear when a 3-layer non-linear projection head [13, 14] is used (instead of the 2-layer projection head).

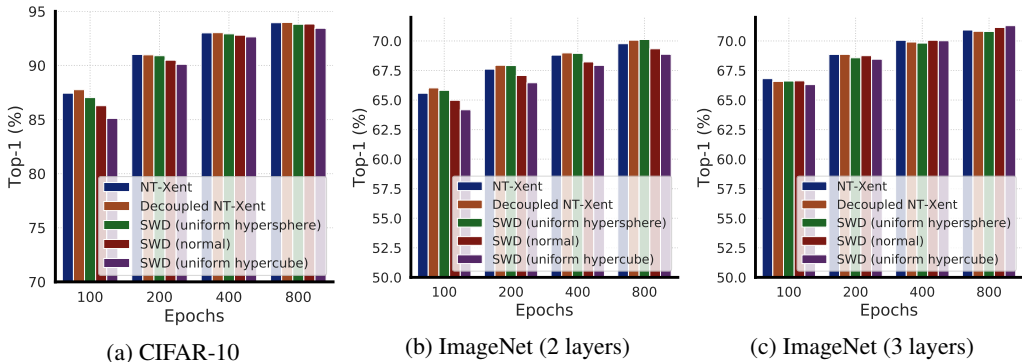


Figure 2: Linear evaluation accuracy of ResNet-50 trained with different losses on CIFAR-10 and ImageNet datasets. For CIFAR-10, the batch size is 128, and a 2-layer projection head is used; for ImageNet, the batch size is 1024, and 2-layer (b) or 3-layer (c) projection heads are used. Numerical results of this Figure (and results with more batch sizes) can be found in Appendix D.

### 2.3 Temperature $\tau$ (in Eq. 2) is (within a range) inversely correlated to weighting $\lambda$ (in Eq. 1)

To see how well the learned distribution matches the prior distribution (e.g. Gaussian), we randomly project the (high-dimensional) representation vectors into 1-d space and plot the histogram distribution. For prior distribution of Gaussian or uniform in hypersphere, these random projections in 1-d space should be Gaussian like.

Figure 3 shows random orthogonal projection of representation from CIFAR-10 test set. We see that both weighting ( $\lambda$  in Eq. 1) and the temperature scaling ( $\tau$  in Eq. 2) have the effect of controlling

distribution matching term, but they have an inverse correlation. This inverse correlation between  $\tau$  and  $\lambda$  is also studied for decoupled NT-Xent loss in Appendix A.

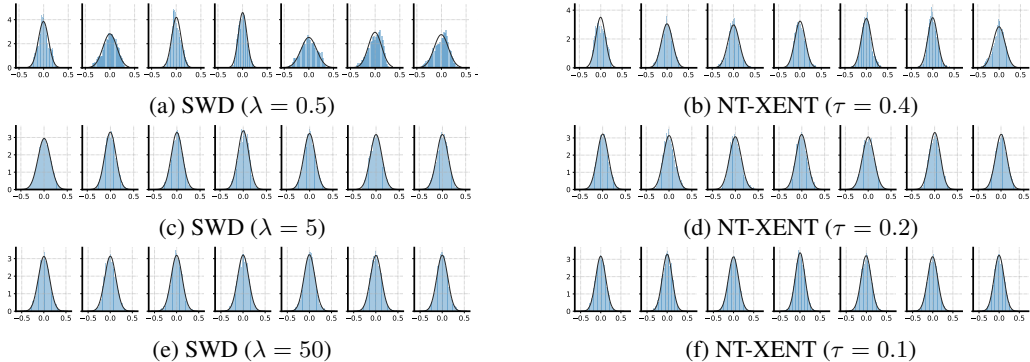


Figure 3: Distribution of random orthogonal projection of output vectors on CIFAR-10 test set (each small plot has its own random projection direction). For SWD (uniform hypersphere) loss, distribution becomes more Gaussian as  $\lambda$  increases. For NT-Xent loss, the distribution becomes more Gaussian as  $\tau$  decreases.

### 3 Feature Suppression

As shown in SimCLR [13, 14], contrastive learning requires good design of data augmentation to work well. One functionality of data augmentation is to remove “easy-to-learn” but less transferable features for the contrastive loss. For example, in certain datasets (e.g. CIFAR/ImageNet where each image has a major object), “color distribution” and “object class” are features likely shared between two augmented views when random cropping is used as augmentation. As shown in [13], without color distortion that randomly shift color distribution while maintaining information regarding object class, the quality of learned representations are significantly worse (evaluated with a linear classifier). In other words, the presence of “color distribution” features suppress its competing feature of “object class”. Here we quantitatively study the feature suppression phenomenon by constructing datasets with explicit and controllable competing features.

#### 3.1 Datasets with explicit and controllable competing features

We propose two strategies to inject competing features to an existing image dataset. One strategy is *channel addition* that add information to the existing RGB channels, and the other strategy is *channel concatenation* that expand the original RGB channels to include additional features. We elaborate them with two concrete examples below.

**DigitOnImageNet dataset.** We overlay MNIST digits on ImageNet images via channel addition/summation (Figure 4a). For each ImageNet image, we assign an unique MNIST digit and replicate it in nine fixed locations, before the standard SimCLR augmentations [13] are applied to create augmented views. So the original ImageNet images and added MNIST digits are competing features. Although it is difficult to quantify information in MNIST digits, we can manually control the number of unique MNIST digits used. Ideally, we want the model to learn both set of features so that it could perform well for both MNIST digit and ImageNet object recognition.

**RandBit dataset.** We concatenate a real image with an image of a random integer in their channel dimension (Figure 4b). The random integer is randomly sampled from range of  $[1, \log_2(n)]$  where  $n$  is a parameter to control. It is replicated across spatial dimension (i.e. all pixel location shares the same value), and it is also represented as  $n$  binary bits/channels instead of a integer or floating number to make it easily learnable. Furthermore, unlike RGB channels, these additional channels of random bits will *not* be augmented so they are identical for both augmented views of the same image. The RGB channels and added channels of random bits are competing features, and this construction allows us to control the amount of information in the added competing feature, which is  $n$  bits. And we know that the mutual information between two views given this construction is at least  $\log_2(n)$ .



(a) ImageNet images overlaid with MNIST digits. The left most column is original image, and others are augmented views via random crop and color distortion. MNIST digits and ImageNet classes are competing features. We vary the number of unique MNIST digits to control the competing features.



(b) Images (of RGB channels) are concatenated with additional channels of random integer sampled from range of  $[1, \log_2(n)]$ . The integer, shared between two views, is replicated for spatial dimension and represented as  $n$  binary channels. RGB channels and random bits are competing features.

Figure 4: Two probing datasets with explicit and controllable competing features.

### 3.2 The strong suppression effect among competing features

For DigitOnImageNet datasets, we vary the number of unique MNIST digits used in the training set, and all MNIST digits are used in the validation/test set. Firstly, we train supervised ResNet-50 on the created datasets with ImageNet labels, and the number of unique MNIST digits has little impact on the top-1 ImageNet classification accuracy (Figure 5b). We then train SimCLR on the datasets with different temperatures. As shown in Figure 5a, when we increase the number of unique MNIST digits, the linear evaluation performance of the learned features for MNIST classes increases accordingly, while that for ImageNet classes decreases significantly. The trade-off between digit recognition ability and object recognition ability shows simple features suppress the learning of hard features shared between two augmented views, and it is difficult to learn both of the competing features using existing contrastive loss (as in SimCLR). Different batch sizes and projection head depths are studied in Appendix C.2, and they have negligible influence to the outcome we observe here.

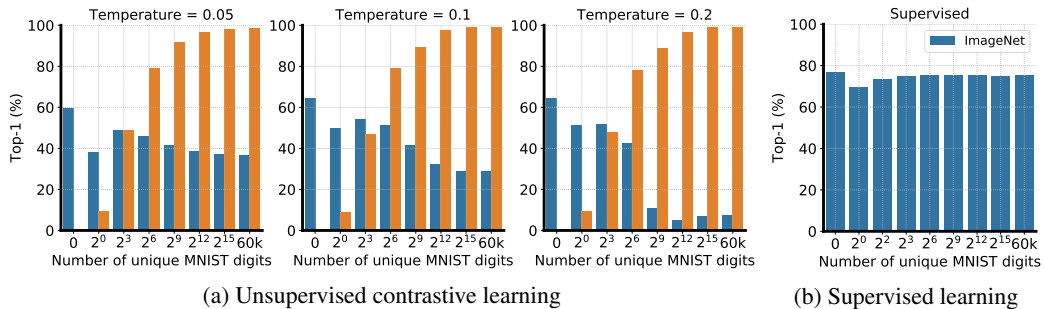
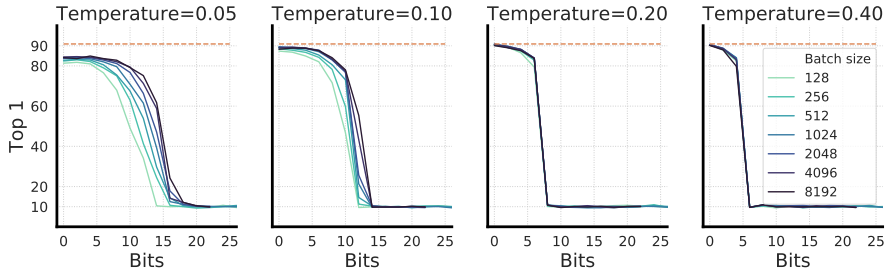
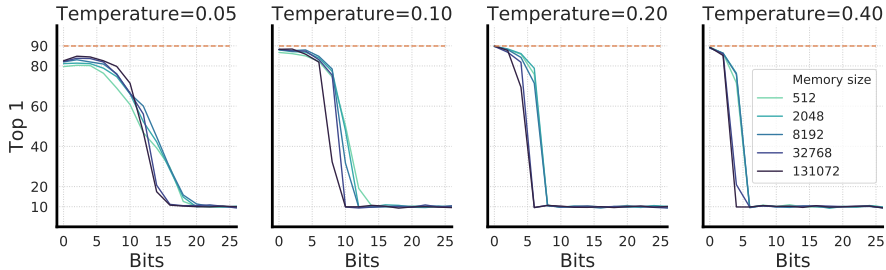


Figure 5: (a) Linear evaluation of learned features for both MNIST classification and ImageNet classification on the DigitOnImageNet dataset. (b) Supervised learning accuracy on ImageNet classification. Batch size of 1024 and 2-layer projection head is used here. Different batch sizes and projection head layers have negligible influence on the trade-off between ImageNet vs MNIST accuracy (see Appendix C.2).

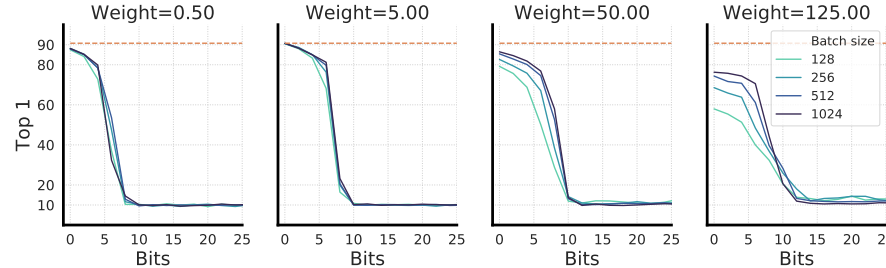
For RandBit dataset, we perform experiments on three different base datasets (on which we add additional channels of random bits), namely MNIST, CIFAR-10, as well as ImageNet. Figure 6 shows linear evaluation on CIFAR-10 with different random bits added (the actual bits are smaller due to collision of sampling, see Appendix C.1 for explanation). We observe that the linear evaluation accuracy decreases quickly with a few bits of the extra channel competing feature added. And this detrimental effect of representation quality cannot be avoided by different contrastive loss functions, batch sizes, as well as memory mechanism in momentum contrast [10]. Although a smaller temperature ( $\tau$ ) or larger weighting ( $\lambda$ ) slightly mitigates the degeneration effect, its baseline performance when no extra bits are added is also worse. With less than 15 bits of competing features added, the representation quality degenerates to the level where RGB channels are completely ignored. Results on MNIST and ImageNet (Appendix C.1) show similar conclusions, and additionally: (1) models of different sizes suffer from the same effect, and (2) the extra bits added have little effect on the representation quality when trained with variational autoencoder (VAE) [23, 24] on MNIST, whose loss function is based on reconstruction.



(a) Standard NT-Xent



(b) NT-Xent with Momentum Contrast (MoCo)



(c) SWD (uniform hypersphere)

Figure 6: Linear evaluation accuracy on CIFAR-10 of ResNet-18 (400 epochs) when different random bits are added. For MNIST and ImageNet, results can be found in Appendix C.1.

#### 4 Related Work

Our work studies the contrastive loss based on cross entropy loss [15, 3, 4, 13]. This loss is widely used in recent successful contrastive learning methods [3–14]. In terms of the contrastive loss, our work is perhaps most related to [17], which shows that formulating contrastive loss as alignment



and uniformity in the hypersphere gives similar performance as the standard contrastive loss. We further generalize this factorization, and show other distribution matching losses can be used, and they could achieve similar results. Other than standard contrastive loss that directly utilize negative examples, BYOL [16] demonstrates another way to maintain representation distribution/entropy without directly relying on distribution matching, and SWAV [25] shows clustering-based method equipped with proper data augmentations could also achieve similar performance. We only conduct preliminary experiments of BYOL on RandBit and found that it also suffers from feature suppression as generalized contrastive loss. And it is expected SWAV would exhibit similar behaviors on RandBit as those random bits could fuel representations for perfect clustering.

The connection between contrastive loss and mutual information has been studied before [3, 21]. We show that for the generalized contrastive loss, it can also be related to mutual information. Despite the connection between the contrastive loss to mutual information, it has been pointed out that mutual information estimation may suffer from certain limitations [26, 27]. More importantly, [28, 12] show that higher mutual information does mean better representation quality. In our work, we find adding mutual information bits between two views which are irrelevant to downstream tasks can be harmful for the quality of learned representations. And data augmentation plays an important role at favoring certain bits of mutual information than the others.

There is a growing number of recent work on the topic of understanding contrastive learning, both theoretically [29–33] and empirically [17, 12, 34, 35]. We believe this is still a very open question and could benefit from more future investigation. Finally, the feature suppression effect in unsupervised contrastive learning that we study in this work may also exist in standard supervised learning (“contrastive loss” between examples and class labels), as suggested by [36].

## 5 Discussions

In this work, we first generalize the standard contrastive loss to a broader family of losses, with an abstract form of  $\mathcal{L}_{\text{alignment}} + \lambda\mathcal{L}_{\text{distribution}}$ . We show that the regularization weight  $\lambda$  is (within a range) inversely correlated to temperature  $\tau$  of standard contrastive loss. With a multi-layer non-linear projection head, different variants of generalized contrastive losses perform similarly under linear evaluation protocol.

We then study the feature suppression in contrastive learning. By constructing two datasets with explicit and controllable competing features, our experiments show that a few bits of easy-to-learn features could suppress, or even fully prevent, the learning of other sets of features. This observation persists across different instantiations of contrastive losses, model sizes, and batch sizes (with or without memories), despite it is far less significant in autoencoder based on a reconstruction loss.

The exact cause of feature suppression is not fully understood in this work, we conjecture the following:

- One possibility is that the contrastive loss quickly saturates with a few bits of mutual information in hidden representations learned between two augmented views. This is essentially caused by that the distribution matching loss that saturates quickly with a few bits of entropy (see Appendix B). Even using a huge batch size only helps at roughly log scale. However, reduce the loss saturation itself may not be enough. Our results show that increasing batch size, or using large number of negatives buffered from an EMA network, have little to none effect at preventing detriment.
- Another possibility is that competing features divide the dataset so it make the effective dataset size smaller. This would be evident in the extreme case, where every image has a unique ID that will not be destroyed by the augmentation, then it would be trivial for the model to identify positive pairs correctly. When several examples share an ID, then the model only needs to distinguish among them, a smaller set compared to all examples.

Our results resonate with [13] on the importance of data augmentation for contrastive learning, as it can be used as a critical tool for favoring certain set of competing features than the others. It also raises a question for future research: is there a better learning strategy for reducing feature suppression effect while relying less on hand-crafted / heuristic-based augmentations?



## Acknowledgements

We specially thank Geoffrey Hinton for many inspiring discussions and helpful advice. We would also like to thank David Fleet, Simon Kornblith, Mohammad Norouzi, Kevin Swersky and Katherine Hermann for insightful discussions. In addition, we are thankful to William Chan and Sara Sabour for ideas on implementation of sorting on TPUs.

## References

- [1] Suzanna Becker and Geoffrey E Hinton. Self-organizing neural network that discovers surfaces in random-dot stereograms. *Nature*, 355(6356):161–163, 1992.
- [2] Alexey Dosovitskiy, Jost Tobias Springenberg, Martin Riedmiller, and Thomas Brox. Discriminative unsupervised feature learning with convolutional neural networks. In *Advances in neural information processing systems*, pages 766–774, 2014.
- [3] Aaron van den Oord, Yazhe Li, and Oriol Vinyals. Representation learning with contrastive predictive coding. *arXiv preprint arXiv:1807.03748*, 2018.
- [4] Zhirong Wu, Yuanjun Xiong, Stella X Yu, and Dahua Lin. Unsupervised feature learning via non-parametric instance discrimination. In *Proceedings of the IEEE Conference on Computer Vision and Pattern Recognition*, pages 3733–3742, 2018.
- [5] R Devon Hjelm, Alex Fedorov, Samuel Lavoie-Marchildon, Karan Grewal, Phil Bachman, Adam Trischler, and Yoshua Bengio. Learning deep representations by mutual information estimation and maximization. *arXiv preprint arXiv:1808.06670*, 2018.
- [6] Philip Bachman, R Devon Hjelm, and William Buchwalter. Learning representations by maximizing mutual information across views. In *Advances in Neural Information Processing Systems*, pages 15509–15519, 2019.
- [7] Olivier J Hénaff, Ali Razavi, Carl Doersch, SM Eslami, and Aaron van den Oord. Data-efficient image recognition with contrastive predictive coding. *arXiv preprint arXiv:1905.09272*, 2019.
- [8] Yonglong Tian, Dilip Krishnan, and Phillip Isola. Contrastive multiview coding. *arXiv preprint arXiv:1906.05849*, 2019.
- [9] Ishan Misra and Laurens van der Maaten. Self-supervised learning of pretext-invariant representations. *arXiv preprint arXiv:1912.01991*, 2019.
- [10] Kaiming He, Haoqi Fan, Yuxin Wu, Saining Xie, and Ross Girshick. Momentum contrast for unsupervised visual representation learning. *arXiv preprint arXiv:1911.05722*, 2019.
- [11] Junnan Li, Pan Zhou, Caiming Xiong, Richard Socher, and Steven CH Hoi. Prototypical contrastive learning of unsupervised representations. *arXiv preprint arXiv:2005.04966*, 2020.
- [12] Yonglong Tian, Chen Sun, Ben Poole, Dilip Krishnan, Cordelia Schmid, and Phillip Isola. What makes for good views for contrastive learning. *arXiv preprint arXiv:2005.10243*, 2020.
- [13] Ting Chen, Simon Kornblith, Mohammad Norouzi, and Geoffrey Hinton. A simple framework for contrastive learning of visual representations. *arXiv preprint arXiv:2002.05709*, 2020.
- [14] Ting Chen, Simon Kornblith, Kevin Swersky, Mohammad Norouzi, and Geoffrey Hinton. Big self-supervised models are strong semi-supervised learners. *arXiv preprint arXiv:2006.10029*, 2020.
- [15] Kihyuk Sohn. Improved deep metric learning with multi-class n-pair loss objective. In *Advances in neural information processing systems*, pages 1857–1865, 2016.
- [16] Jean-Bastien Grill, Florian Strub, Florent Alché, Corentin Tallec, Pierre H. Richemond, Elena Buchatskaya, Carl Doersch, Bernardo Avila Pires, Zhaohan Daniel Guo, Mohammad Gheshlaghi Azar, Bilal Piot, Koray Kavukcuoglu, Rémi Munos, and Michal Valko. Bootstrap your own latent: A new approach to self-supervised learning, 2020.
- [17] Tongzhou Wang and Phillip Isola. Understanding contrastive representation learning through alignment and uniformity on the hypersphere. *arXiv preprint arXiv:2005.10242*, 2020.

- [18] Julien Rabin, Gabriel Peyré, Julie Delon, and Marc Bernot. Wasserstein barycenter and its application to texture mixing. In *International Conference on Scale Space and Variational Methods in Computer Vision*, pages 435–446. Springer, 2011.
- [19] Nicolas Bonneel, Julien Rabin, Gabriel Peyré, and Hanspeter Pfister. Sliced and radon wasserstein barycenters of measures. *Journal of Mathematical Imaging and Vision*, 51(1):22–45, 2015.
- [20] Soheil Kolouri, Kimia Nadjahi, Umut Simsekli, Roland Badeau, and Gustavo Rohde. Generalized sliced wasserstein distances. In *Advances in Neural Information Processing Systems*, pages 261–272, 2019.
- [21] Ben Poole, Sherjil Ozair, Aaron van den Oord, Alexander A Alemi, and George Tucker. On variational bounds of mutual information. *arXiv preprint arXiv:1905.06922*, 2019.
- [22] Kaiming He, Xiangyu Zhang, Shaoqing Ren, and Jian Sun. Deep residual learning for image recognition. In *Proceedings of the IEEE conference on computer vision and pattern recognition*, pages 770–778, 2016.
- [23] Diederik P Kingma and Max Welling. Auto-encoding variational bayes. *arXiv preprint arXiv:1312.6114*, 2013.
- [24] Danilo Jimenez Rezende, Shakir Mohamed, and Daan Wierstra. Stochastic backpropagation and approximate inference in deep generative models. *arXiv preprint arXiv:1401.4082*, 2014.
- [25] Mathilde Caron, Ishan Misra, Julien Mairal, Priya Goyal, Piotr Bojanowski, and Armand Joulin. Unsupervised learning of visual features by contrasting cluster assignments. *arXiv preprint arXiv:2006.09882*, 2020.
- [26] David McAllester and Karl Stratos. Formal limitations on the measurement of mutual information. In *International Conference on Artificial Intelligence and Statistics*, pages 875–884, 2020.
- [27] Jiaming Song and Stefano Ermon. Understanding the limitations of variational mutual information estimators. *arXiv preprint arXiv:1910.06222*, 2019.
- [28] Michael Tschannen, Josip Djolonga, Paul K Rubenstein, Sylvain Gelly, and Mario Lucic. On mutual information maximization for representation learning. *arXiv preprint arXiv:1907.13625*, 2019.
- [29] Sanjeev Arora, Hrishikesh Khandeparkar, Mikhail Khodak, Orestis Plevrakis, and Nikunj Saunshi. A theoretical analysis of contrastive unsupervised representation learning. *arXiv preprint arXiv:1902.09229*, 2019.
- [30] Yao-Hung Hubert Tsai, Yue Wu, Ruslan Salakhutdinov, and Louis-Philippe Morency. Demystifying self-supervised learning: An information-theoretical framework. *arXiv preprint arXiv:2006.05576*, 2020.
- [31] Christopher Tosh, Akshay Krishnamurthy, and Daniel Hsu. Contrastive learning, multi-view redundancy, and linear models. *arXiv preprint arXiv:2008.10150*, 2020.
- [32] Yuandong Tian, Lantao Yu, Xinlei Chen, and Surya Ganguli. Understanding self-supervised learning with dual deep networks. *arXiv preprint arXiv:2010.00578*, 2020.
- [33] Jason D Lee, Qi Lei, Nikunj Saunshi, and Jiacheng Zhuo. Predicting what you already know helps: Provable self-supervised learning. *arXiv preprint arXiv:2008.01064*, 2020.
- [34] Nanxuan Zhao, Zhirong Wu, Rynson WH Lau, and Stephen Lin. What makes instance discrimination good for transfer learning? *arXiv preprint arXiv:2006.06606*, 2020.
- [35] Senthil Purushwalkam and Abhinav Gupta. Demystifying contrastive self-supervised learning: Invariances, augmentations and dataset biases. *arXiv preprint arXiv:2007.13916*, 2020.
- [36] Katherine L Hermann and Andrew K Lampinen. What shapes feature representations? exploring datasets, architectures, and training. *arXiv preprint arXiv:2006.12433*, 2020.

## A The inverse correlation between $\tau$ and $\lambda$ in decoupled NT-xent loss (Eq. 4)

Here we tune  $\tau$  and  $\lambda$  separately for the decoupled NT-xent loss (Eq. 4). Figure A.1 shows the linear evaluation of ResNet-18 trained in 200 epochs. We see that the temperature  $\tau$  and the weighting  $\lambda$  are inversely correlated for most range. In practice one could simply fix one and tune the other.

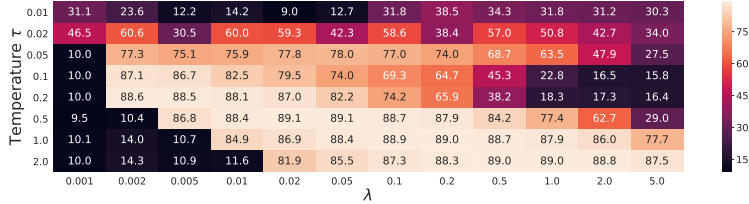


Figure A.1: Linear evaluation of ResNet-18 trained on CIFAR-10 (200 epochs) using decoupled NT-Xent loss (Eq. 4). The temperature  $\tau$  and the weighting  $\lambda$  are mostly inverse correlated.

## B Distribution matching loss, LogSumExp or SWD, saturate with a few bits of entropy

Here we study the saturation of distribution matching loss (based on LogSumExp or SWD), without presence of the alignment term. To do so, we create square images with  $k$  binary channels (instead of RGB channels), and all pixels at different locations of a  $32 \times 32$  image share the same value, this allows us to use the same architecture as one for CIFAR-10 (i.e. ResNet-18 and 2-layer projection head with output dimensionality of 64). We note that this experiment can also be conducted on images of  $1 \times 1$  size with other architecture. It is not difficult to see the entropy of this dataset is  $k$  bits. A mini-batch of data points (without augmentations) are first encoded via the network, and then the distribution matching loss is defined on the network's outputs. The network is trained for 400 epochs, and longer training epochs makes little difference. Figure B.1 shows that distribution loss saturates quickly with a few bits of entropy in the dataset (same or less bits in representations), and both temperature and batch sizes have effects on the saturation behavior.

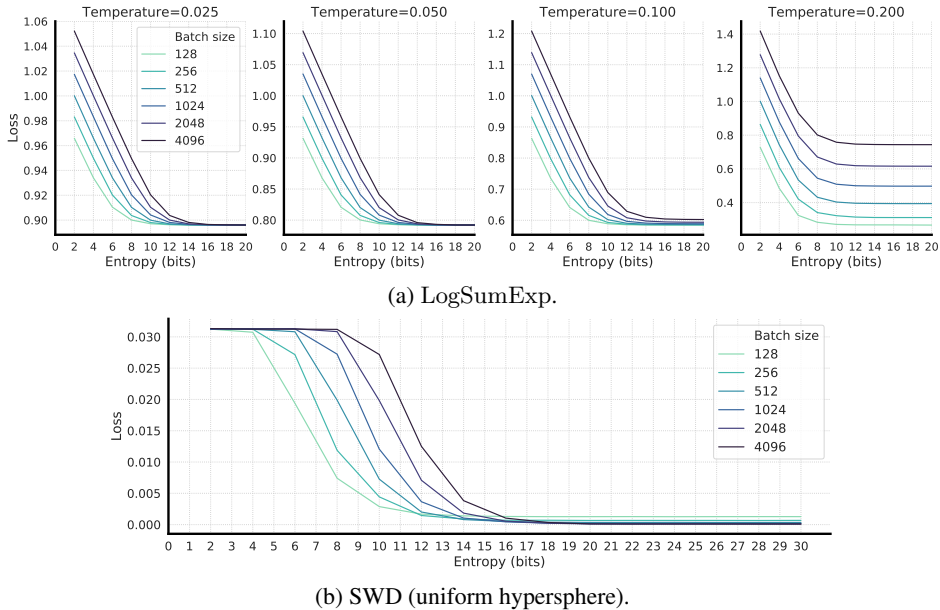


Figure B.1: Distribution matching loss saturates quickly with a few bits of entropy. The saturation varies slightly across batch sizes.

## C Extra results on probing datasets with competing features

### C.1 Extra results on RandBit dataset based on CIFAR-10

Figure C.1 shows the linear evaluation accuracy of models trained on MNIST and ImageNet (with additional random bits added). For MNIST, we also evaluate variational autoencoder (VAE) [23, 24] whose loss function is based on reconstruction. As shown in Figure C.1b, the extra bits added have little effect on the linear evaluation performance of the learned features.

It is worth noting that the bits in the x-axis are computed based on how random integers are sampled for each image. However, this is an overestimation of actual bits as there are collision in generated integers.

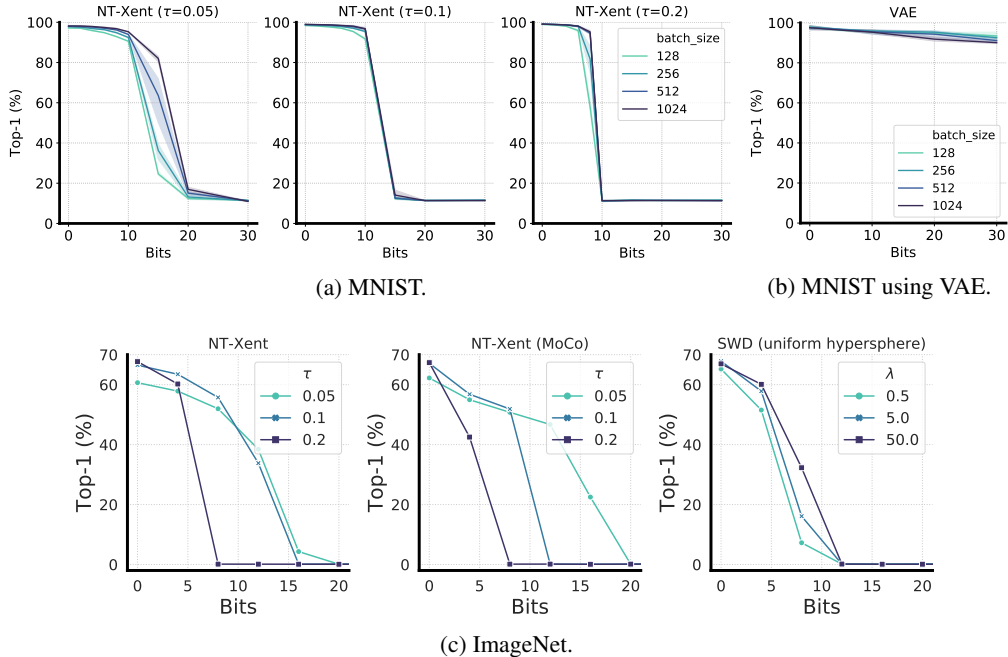


Figure C.1: Linear evaluation of learned features when a few bits of competing features added. (a) and (b) are results on MNIST using contrastive learning or generative modeling (i.e. VAE); results are averaged over different model sizes. (c) is result on ImageNet with different losses (including memory mechanism in MoCo).

### C.2 Extra results on DigitOnImageNet dataset

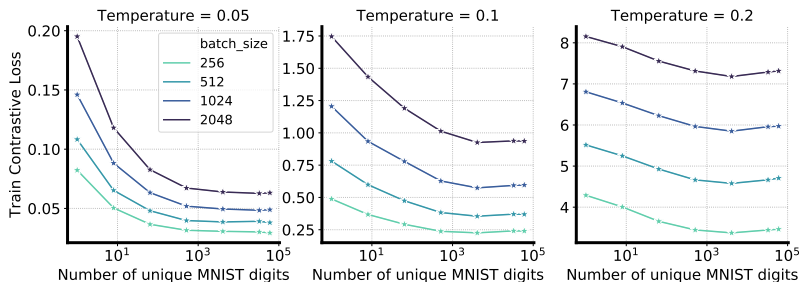


Figure C.2: Training contrastive loss when different number of MNIST digits are added (corresponding to experiments reported in Figure 5 and Figure C.3).

Figure C.2 show the training contrastive losses corresponding to experiments reported in Figure 5. We see that by adding more MNIST digits, the contrastive loss turn to decrease, though at different amount for varying temperatures.

Figure C.3 and C.4 show that both batch sizes as well as projection head has negligible influences on the learned representations when competing features are added.

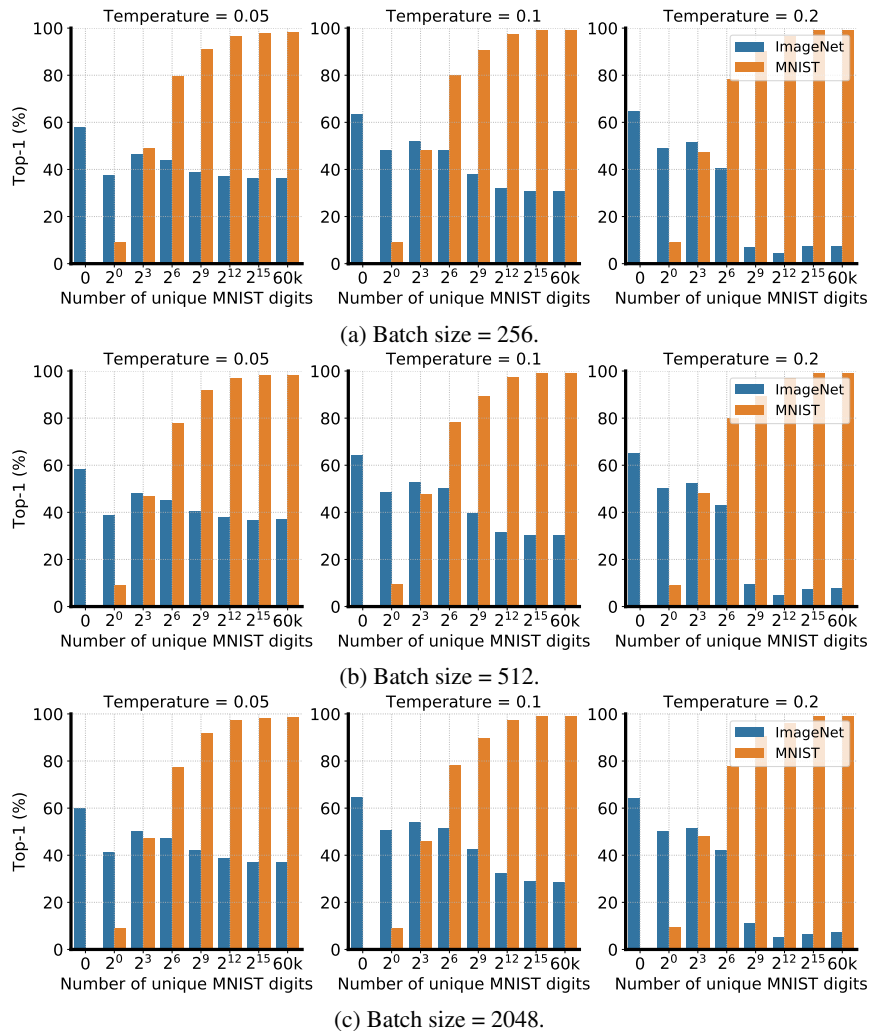


Figure C.3: Linear evaluation of ImageNet classification and MNIST classification on the DigitOn-ImageNet dataset. Different batch sizes are tested, and they have negligible influences on results.

## D Linear evaluation of generalized contrastive loss on CIFAR-10 and ImageNet

Table D.1, D.2 and D.3 show linear evaluation performance of ResNet-50 trained with different losses (numerical results of Figure 2). Similar to [13, 14], a square root learning rate is used. In addition, results of different batch sizes are also compared, and we find the differences are small with reasonable sizes (e.g. 128 for CIFAR-10 and 1024 for ImageNet).

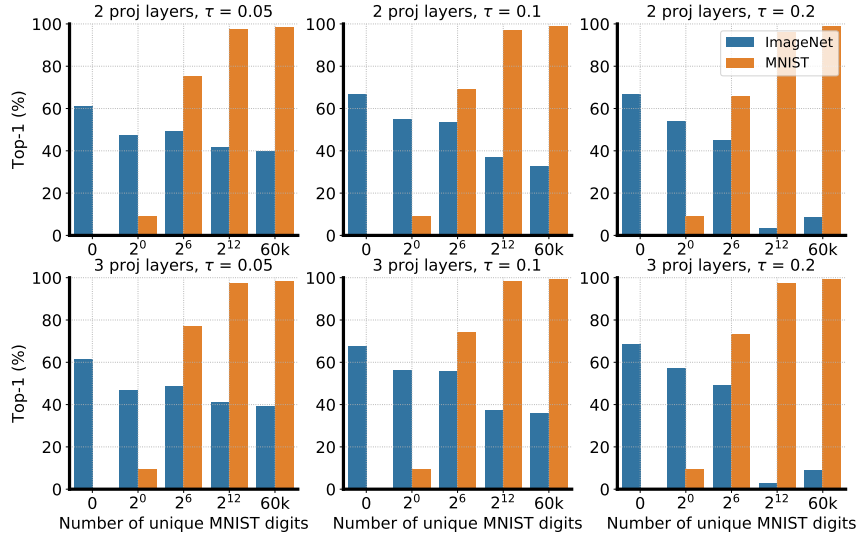


Figure C.4: Linear evaluation of ImageNet classification and MNIST classification on the DigitOn-ImageNet dataset. Different projection head depths are tested, and they have negligible influences on results.

Table D.1: Linear evaluation accuracy (top-1) of ResNet-50 trained with different losses on CIFAR-10.

Loss	Epoch Batch size	100	200	400	800
NT-Xent	128	87.4	91.0	93.0	93.9
	256	88.0	91.3	93.0	93.6
	512	87.9	91.3	92.9	93.7
	1024	88.2	91.2	92.7	93.3
Decoupled NT-Xent	128	87.8	91.0	93.0	94.0
	256	87.7	91.1	92.8	93.6
	512	87.5	91.3	92.7	93.6
	1024	87.5	91.0	92.6	93.7
SWD (normal)	128	86.3	90.5	92.8	93.8
	256	86.2	90.8	93.1	94.1
	512	85.0	90.7	92.9	94.1
	1024	83.3	89.9	93.0	93.9
SWD (uniform hypercube)	128	85.1	90.1	92.6	93.4
	256	84.6	89.9	92.9	93.8
	512	83.1	89.8	92.8	93.8
	1024	81.3	88.3	92.2	93.6
SWD (uniform hypersphere)	128	87.0	90.9	92.9	93.8
	256	87.1	90.9	92.5	93.7
	512	86.6	90.8	92.9	93.4
	1024	86.0	90.3	92.5	93.2

Table D.2: Linear evaluation accuracy (top-1) of ResNet-50 trained with different losses on ImageNet (with 2-layer projection head).

Loss	Epoch Batch size	100	200	400	800
NT-Xent	512	65.4	67.3	68.7	69.3
	1024	65.6	67.6	68.8	69.8
	2048	65.3	67.6	69.0	70.1
Decoupled NT-Xent	512	65.8	67.6	68.9	69.5
	1024	66.0	67.9	69.0	70.1
	2048	65.8	67.9	69.3	70.2
SWD (normal)	512	64.9	66.8	68.0	69.0
	1024	65.0	67.1	68.2	69.3
	2048	65.0	66.9	68.4	69.7
SWD (uniform hypercube)	512	64.3	66.4	67.8	68.7
	1024	64.2	66.5	67.9	68.9
	2048	63.9	66.6	67.9	69.0
SWD (uniform hypersphere)	512	65.6	67.7	69.0	70.0
	1024	65.8	67.9	69.0	69.6
	2048	65.6	67.8	69.2	69.8

Table D.3: Linear evaluation accuracy (top-1) of ResNet-50 trained with different losses on ImageNet (with 3-layer projection head).

Loss	Epoch Batch size	100	200	400	800
NT-Xent	512	66.6	68.4	70.0	71.0
	1024	66.8	68.9	70.1	70.9
	2048	66.8	69.1	70.4	71.3
Decoupled NT-Xent	512	66.8	68.4	69.6	70.6
	1024	66.6	68.9	69.9	70.8
	2048	66.6	69.0	70.1	70.8
SWD (normal)	512	66.5	68.4	69.8	70.8
	1024	66.6	68.8	70.1	71.1
	2048	66.7	69.1	70.2	71.1
SWD (uniform hypercube)	512	66.1	68.3	69.7	70.7
	1024	66.3	68.5	70.0	71.3
	2048	65.8	68.2	70.1	71.1
SWD (uniform hypersphere)	512	66.5	68.3	69.5	70.5
	1024	66.6	68.6	69.8	70.8
	2048	66.5	68.7	70.2	70.9